Article

The Effect of SiC on the Phase Composition and Structure of Mixed Slag

Shuai Hao, Guoping Luo *, Yuanyuan Lu, Shengli An [ID], Yifan Chai and Wei Song

School of Materials and Metallurgy, Inner Mongolia University of Science and Technology, Baotou 014010, China; haoshuai@stu.imust.edu.cn (S.H.); m15024704269@163.com (Y.L.); san@imust.edu.cn (S.A.); chaiyifan@live.cn (Y.C.); qiangwei_1205@126.com (W.S.)
* Correspondence: luoguoping3@126.com

Abstract: In order to investigate the influence of SiC on the composition and structure of mixed slag (blast-furnace slag: steel slag = 1:9), the chemical composition, equilibrium-phase composition, and microscopic morphological characteristics and elemental distribution in the microscopic region of the SiC-reagent-tempered slag samples were analyzed by X-ray diffractometer (XRD), FactSage7.1 thermodynamic analysis software, scanning electron microscope, and energy spectrum analyzer. It was found that the main physical phases of the tempered slag samples were magnesia–silica–calcite ($Ca_3Mg(SiO_4)_2$, C_3MS_2), calcium–aluminum yellow feldspar ($Ca_2Al_2SiO_7$, C_2AS), C_2S, and iron alloy. Theoretical calculations suggest that the experimental temperature should be higher than 1500 °C to facilitate the combination of P^{5+} with Fe and Mn in the liquid phase to form an alloy, reduce the P5+ content in the tempered slag, and create conditions for the self-powdering of the conditioned slag. The doping of the SiC reagent can increase the liquid phase line temperature and reduce the binary basicity in the liquid phase; the liquid phase line temperatures were 1150 °C, 1200 °C, and 1300 °C and the basicities in the liquid phase were 4.68, 4.13, and 3.10 for the doping amounts of 3%, 4%, and 5% of the SiC reagent, respectively. The mixed slag doped with 4% SiC reagent achieves self-powdering and reduction of ferroalloys during the air-cooling and cooling processes, realizing the purpose of "resource utilization" of blast-furnace slag and steel slag.

Keywords: steel slag; blast-furnace slag; SiC reagent; high-temperature tempering; XRD; FactSage7.1; self-powdering

1. Introduction

The steel industry is the pillar industry of China's national economy. Since 1996, when China's steel production exceeded 100 million tons for the first time, China's steel industry has entered a rapid development track. Steel production has always ranked first in the world [1]. Steel slag is a by-product of the steelmaking process and a bulk solid waste resource of the metallurgical process, accounting for about 12%~15% of steel production. In 2021, China's crude-steel production reached 1.03 billion tons and steel-slag production was about 130 million tons. The accumulation of metallurgical slag in Chinese metallurgical enterprises has exceeded 2 billion tons and is accumulating at an annual increment of about 100 million tons, of which about 80% is converter steel slag [2]. As a silicate by-product of the high-temperature steelmaking process, the chemical composition and mineral composition of converter steel slag is similar to that of cement and concrete admixtures [3], and, if it can be converted into slag micronized powder, its scale and resource utilization in the construction field can be realized. However, due to the high iron content of converter steel slag [4] and its hard texture, its crushing and fine grinding into steel-slag micronized powder will significantly increase the cost of recycling [5]. In the comprehensive utilization of steel slag, China still has a generally low utilization rate, limited by the use of a single method and other problems [6]. The steel slag discharged

from 11 bases of Baogang Huanke in 2020 amounted to 14.39 million tons of steel slag. Its utilization rate was 99%, with use in the construction field accounting for a large part. 65% of this was used in cement–concrete mix, asphalt concrete, and foundations, and road-base treatment accounted for 18%. In addition, waste steel slag crushing and screening can be used as the main aggregate for brick-making, which can result in permeable bricks, imitation-stone bricks, curb bricks, slope bricks, blocks, and other products; these products can be widely used in municipal squares, landscaping, highways, and other projects, both to achieve the recycling of steel slag, and also to create economic benefits for enterprises [7]. However, due to the high iron content and hard texture of converter slag, its crushing and fine grinding into steel slag micronized powder significantly increases the cost of recycling. The self-powdering of steel slag is a key technology to realize low-cost steel-slag powder production and large-scale utilization. The volume expansion (11% expansion) and natural pulverization caused by the crystallographic transformation of calcium orthosilicate ($2CaO\text{-}SiO_2$, C_2S) during the cooling of steel slag (transformation of $\beta\text{-}2CaO\text{-}SiO_2$ to $\gamma\text{-}2CaO\text{-}SiO_2$ occurs upon cooling to 725 °C) can be utilized to produce low-cost steel-slag micronized powder, which is of great significance for the large-scale utilization of steel slag [8,9]. Related studies have shown that high-basicity steel slag has low calcium silicate content, which is not conducive to steel-slag self-powdering. Lower basicity is beneficial to the realization of steel-slag self-powdering, while blast-furnace slag as a by-product of iron-making, has a water-quenched slag basicity of around 1.0 and can be used as a steel-slag tempering agent, which can not only reduce the basicity of steel slag, but promote the generation of C_2S and C_3S with better cementing activity [10], and improve the cementing activity of steel slag. To melt blast-furnace slag, the steel slag is tempered to eliminate unstable factors, such as f-CaO and f-MgO, in the steel slag. From the analysis of the physical composition of steel slag, we found that the impact of steel slag self-powdering was in addition to its basicity for two other reasons [11]; on the one hand, due to the high content of iron oxides in the slag, the solid solution of iron and magnesium (MgO-2FeO), magnesium ferrate ($MgO \cdot Fe_2O_3$), and calcium iron aluminate ($Ca_2(Al,Fe)_2O_5$) reduces the precipitation of calcium orthosilicate, which plays a suppressive role in the steel slag self-powdering; on the other hand, because the steel slag contains a certain amount of phosphorus oxide, the phosphorus ion P^{5+} will be solidly soluble in calcium orthosilicate crystals during solidification, which plays a role in stabilizing $\beta\text{-}C_2S$ crystals, inhibiting the crystalline transformation of $\beta\text{-}C_2S$ to $\gamma\text{-}C_2S$ and hindering the self-powdering of the steel slag. Combined with the chemical composition of the slag, and away from the high-temperature environment, the use of the SiC reagent [12] with high melting point characteristics (SiC melting point > 2700 °C), with a graphite crucible reduction of mixed slag tempering (tempering slag), both are conducive to the reduction of iron oxides in the tempering slag and the removal of phosphorus oxides, but also the reduction of basicity ($R_2 = \frac{\omega(CaO)}{\omega(SiO_2)}$) of the tempering slag, to promote the occurrence of self-powdering of the tempering slag. After pulverization of the tempered slag in $\gamma\text{-}C_2S$, there is a high rate of carbonation reaction [13] if the appropriate particle size of the calcium silicate mixed with water in a maintained CO_2 atmosphere can produce a high-strength structural material with cementation characteristics, especially if the CO_2 partial pressure is high enough, and this point can be reached in a few hours and even exceed the standard maintenance days of the index of ordinary cement. Therefore, if we can develop a high-efficiency, low-cost steel slag self-powdering technology to achieve energy reuse, the development of steel enterprise has a pivotal role.

2. Materials and Methods

2.1. Experimental Materials

In this experiment, Baogang steel slag and water-quenched blast-furnace slag are used as raw materials, and Purity 99% silicon carbide (Macklin, Shanghai Chemical Industry Park, Shanghai, China) pure reagents are added in the form of external admixture, whose chemical composition is shown in Table 1.

Table 1. Chemical composition of blast-furnace slag and steel slag (mass fraction, %).

Sample Name	$w(Fe_2O_3)$	$w(CaO)$	$w(SiO_2)$	$w(Al_2O_3)$	$w(P_2O_5)$	$w(MgO)$
Blast-furnace slag	1.64	41.05	31.52	13.92	—	8.26
Steel slag	17.23	43.02	13.16	3.26	1.50	7.22
Mixed slag	3.07	42.82	15.00	4.33	1.35	7.32

2.2. FactSage7.1 Parameter-Setting Conditions

The Equilib module in FactSage7.1 was used to calculate the phase composition of 100 g slag at equilibrium under different temperature conditions and to analyze the variation law of its phase composition. The specific parameter conditions are shown in Table 2.

Table 2. Parameters setting of FactSage7.1.

Database	FToxid7.1, FactPS7.1
Base-Phase	Slag, clinopyroxene, monoxide, liquid, oxides, spinel, wollastonite, bC_2S, aC_2S, melilite, olivine

2.3. Experimental Protocol

First, steel slag, and blast-furnace slag were crushed by a crusher and sieved by mesh sieve (−0.074 mm). The blast-furnace slag and steel slag were mixed at a mass ratio of 1:9, mixed with 3%, 4%, and 5% SiC reagents, respectively, and then they were loaded into the mixing tank, mixed on the mixer (time: 2 h), and taken out for use. Next, the slag sample was placed in the graphite crucible and placed into the KTF-1700-VT high-temperature vertical furnace with a heating system of 10 °C/min from room temperature to 1000 °C, and then with a heating system of 5 °C/min from 1000 °C to 1550 °C, holding the temperature for 1 h, then the furnace was cooled to 1000 °C and the slag sample removed, air-cooled, and cooled to room temperature. Finally, an appropriate amount of the roasted specimen was taken, ground to a powder (≤0.074 mm), and subjected to a D8-advanced X-ray diffractometer (Germany Brock, Ostbevern, Germany) with the setting conditions of Cu-Kα as target, scanning range of 20~80°, and a speed of 5°/min. Scanning type was as follows: emitter-detection linkage, scanning voltage of 20 kV, and scanning current of 5 mA. The microscopic morphological characteristics and elemental distribution SEM-EDS (Japan Electronics, Tokyo, Japan) in the microscopic region of the roasted specimens were analyzed by scanning electron microscopy and energy-spectrum analyzer.

3. Experimental Results and Discussion

3.1. Macroscopic Morphology of Tempered Slag

The results of SiC reagent tempering modified slag (tempering slag) by high-temperature roasting are shown in Figure 1. From Figure 1a, it can be seen that the tempered slag was doped with 3% SiC, and high-temperature roasting air-cooling did not occur after the natural pulverization phenomenon, but there was the formation of a smooth crust on the surface of the sample and the internal shell of the slag during the local pulverization phenomenon, accompanied by the generation of iron oxides. Analysis showed that: 3% SiC reagent at high-temperature conditions is not able to temper the slag in the iron oxide and phosphorus oxide content to reduce the self-powdering critical conditions below; in the solidification process, it will form more iron and magnesium solid solution (MgO-2FeO), magnesium ferrate ($MgO·Fe_2O_3$), and calcium iron aluminate ($Ca_2(Al, Fe)_2O_5$) to form a slag lump; orthosilicate precipitation is reduced; and C_2S crystalline transformation stress is not enough to produce the tempered slag in the cooling process of self-powdering. From Figure 1b, it can be seen that when the tempering slag is doped with 4% SiC, the air-cooling process occurs during the self-powdering phenomenon, and a round ferroalloy is produced. The analysis suggests that the 4% SiC reagent can reduce the iron oxide and phosphorus

oxide in the tempering slag to below the critical value under high-temperature conditions, and the stress generated by the C_2S crystallographic transformation of the tempering slag during the cooling process makes the self-powdering of the tempering slag occur by volume expansion. According to existing research, the steel slag in the molten state, P^{5+} to C_2S internal enrichment, and the formation of a-C_2S-C_3P in the cooling process inhibits C_2S crystalline transformation; thermodynamic calculations indicate that the steel slag iron oxides, manganese oxides before phosphorus oxides are reduced, with the increase in temperature, P^{5+} ions into the liquid phase and Fe and Mn combination, cooling process in the form of iron alloy and steel slag separation, when the steel slag P_2O_5 content is lower than 0.25%, the effect of P^{5+} on the crystalline transformation of C_2S is small and it does not act as the main factor affecting self-powdering; therefore, it is considered that the doping of 4% SiC reagent can completely reduce the iron oxide and manganese oxide in the tempered slag, and the phosphorus oxide is reduced to less than 0.25%, which is beneficial to the recovery and utilization rate of valuable metals in the tempered slag. From Figure 1c, it can be seen that when the tempering slag is doped with 5% SiC, the air-cooling process triggers the self-powdering phenomenon, but the powdering effect is significantly lower than that of the specimen doped with 4% SiC, and analysis reveals that high-temperature conditions, with the increase in SiC doping, provide favorable conditions for the carbonization reaction of C_2S. The carbonization product is $CaCO_3$ and highly polymerized SiO_2 gel, increasing the stability of the C_2S crystalline form. Therefore, this part of the specimen was not completely pulverized.
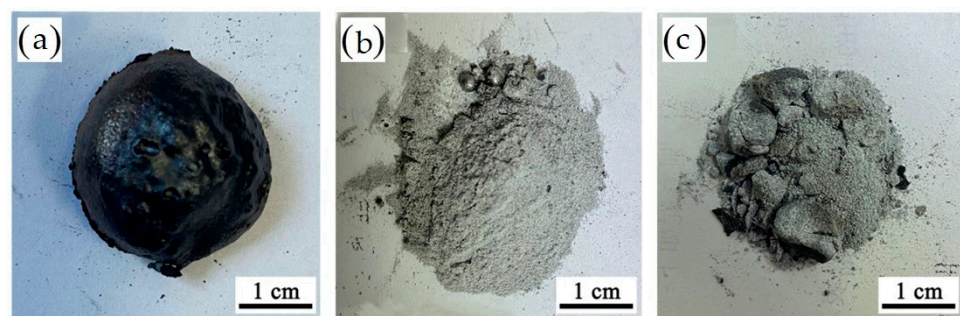

Figure 1. Tempered slag roasted specimens ((**a–c**) mixed with 3%, 4%, 5% SiC reagent slag, defined as S-1, S-2 and S-3).

3.2. Thermodynamic Analysis of Tempered Slag

From the analysis of the direction of crystalline transformation, the transformation process of polycrystalline C_2S structure is a process of changing the arrangement of the spatial structure of the dot matrix. The C_2S crystal phase change process can be regarded as a process of microscopic particle diffusion. If the system liquid phase is insufficient, the transformation of the crystalline shape will be resisted. In order to further clarify the crystalline morphology of C_2S at different temperatures, the FactSage7.1 thermodynamic software Equilib module was used to select the FactPS, FToxid, FTsalt, and FSstel databases to simulate the synthesis of C_2S with n(CaO):n(SiO_2) = 2:1 in steps of 1 °C and analyze the 500~2500 °C C_2S crystalline structure in the equilibrium phase. The calculations reveal that the transition temperature of γ-C_2S to α'_L-C_2S is 847 °C and the temperature starts from 1300 °C. Ca_3SiO_5 is formed in the material phase with 4.95%, and when the temperature is 1437 °C, the point is reached of α'_H-C_2S to α-C_2S crystalline transition. The α-C_2S melting temperature is 2154 °C, but, due to a database problem, the calculations do not indicate the transition temperatures of α'_L-C_2S to α'_H-C_2S nor β-C_2S to γ-C_2S. The crystallographic transition temperatures are shown in Figure 2. The temperature measured by thermodynamics is slightly higher than the crystallographic transition temperature measured by existing studies. The transition between β-C_2S, a monoclinic crystal system

with a bond angle of 94.58°, and γ-C_2S, an orthorhombic crystal system with a bond angle of 90°, results in a change in volume and self-powdering due to the difference in bond angles.
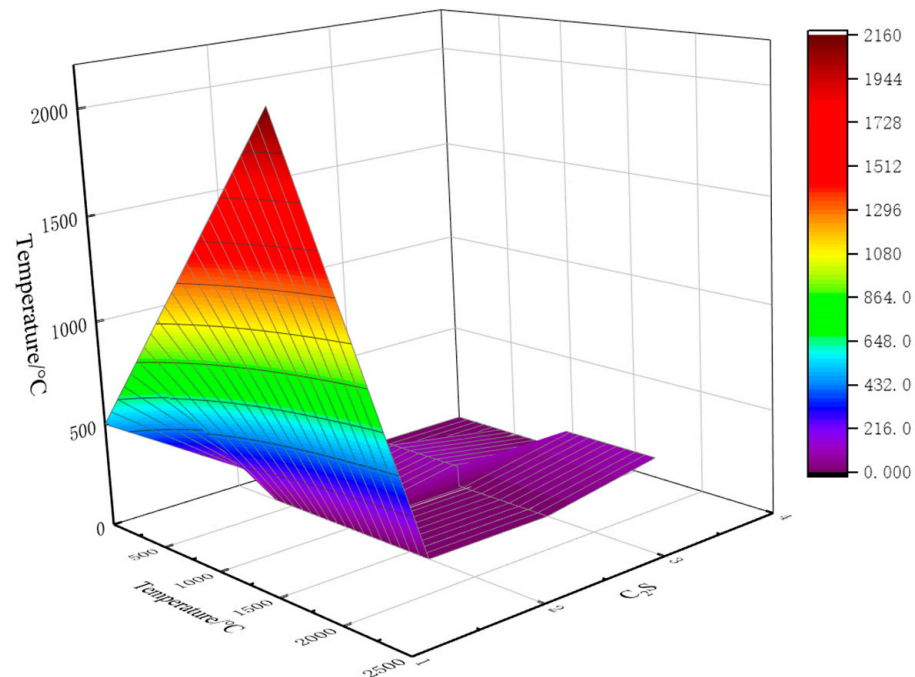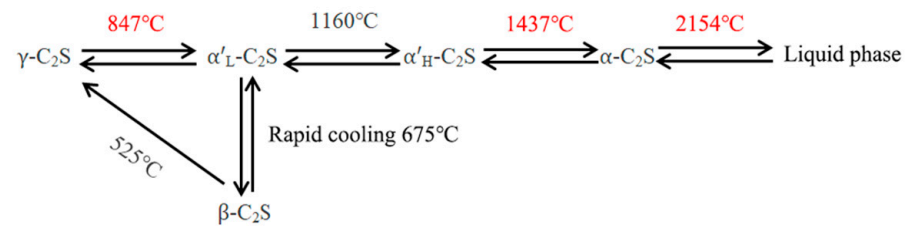

Figure 2. C_2S crystal shape transition with temperature (different colors indicate different temperature ranges).

In order to further explore the change pattern of the material phase of the tempered slag during the warming process, the equilibrium-phase composition of the tempered slag with 3%, 4%, and 5% SiC at different temperatures was simulated using the thermodynamic calculation software FactSage7.1 equilibrium module, and the calculation results are shown in Figure 3. From (a) in Figure 3, it can be seen that the highest percentage of C_2S is found in S-2 at the temperature of 1000 °C, and its percentage is 60.83%, followed by S-1 and S-3, with 56.54% and 49.50%, respectively. With the increase in temperature, the overall C_2S mass proportion showed a decreasing trend, and when the temperature was higher than 1224 °C, the C_2S content proportion in S-2 and S-3 were both higher than that in S-1; near the temperature of 1100 °C, the inflection point of S-1 and S-3 curves appeared, while the inflection point of S-2 curve appeared near 1200 °C. Combined with Figure 3c, it can be seen that the temperature in the range of 1150~1250 °C, S-2 C_2S -C_3P content increases with the increase in temperature, and the percentage of C_2S-C_3P content reaches the highest at the temperature of 1250 °C, which is 20.32%, and, at this time, the percentage of C_2S content in the material phase is 52.03%. This indicates the solid solution of P^{5+} into C_2S and the formation of C_2S-C_3P in the temperature range of 1150~1250 °C. According to the existing studies, it was found that the formation of C_2S-C_3P would inhibit the crystallographic transformation of C_2S from β- C_2S to γ- C_2S and affect the self-powdering of steel slag. S-1 temperature in the temperature range of 1200~1350 °C, the C_2S-C_3P content were lower than 1.00%, and, at this temperature, the C_2S content decreased from 49.57% to 37.96%,

and the analysis combined with Figure 3b suggests that C_2S dissolved into the liquid phase with the increase in temperature. If the temperature is sharply cooled under this temperature condition, it is theoretically easy to realize the self-powdering of the tempered slag. The percentage of C_2S-C_3P content increases faster when the S-3 temperature is in the range of 1250~1350 °C, and the percentage of C_2S-C_3P content reaches the highest at 1350 °C, which is 23.28%, and the percentage of C_2S content increases from 47.66% to 51.32% at this temperature. At this temperature, the self-pulverization of tempered slag is not favorable. At temperatures higher than 1350 °C, the C_2S-C_3P content of S-1 and S-2 increased significantly, and the trend of S-1 growth was significantly stronger than that of S-2. At temperatures higher than 1367 °C, the C_2S-C_3P content of S-1 in the material phase was higher than that of S-2, and at temperatures higher than 1500 °C, the C_2S-C_3P dissolved into the liquid phase, and at 1500 °C, the C_2S content accounted for 32.40% and 40.48%, respectively. When the temperature was higher than 1400~1450 °C, the content of C_2S-C_3P in the physical phase of S-3 was lower than 1.37%. At this time, the percentage of C_2S content was 48.29%, and the temperature was higher than 1450 °C, and C_2S-C_3P dissolved into the liquid phase. From Figure 3b,d, it can be seen that with the increase in SiC doping, the temperatures of the liquid phase produced in S-1, S-2, and S-3 are 1150 °C, 1200 °C, and 1300 °C, respectively, and the basicity in the liquid phase is 4.68, 4.13, and 3.10, respectively, which indicates that the doping of SiC can reduce the melting point of the tempered slag, and, at the same temperature, the amount of material-liquid phase decreases and the kinetic conditions weaken, affecting the pulverization effect. This also explains the reason why the pulverization effect of specimens doped with 3% and 5% SiC reagents in Figure 1 is significantly weaker than that of specimens doped with 4% SiC reagents. From Figure 3e, it can be seen that the percentage of Fe content in the material phase increases significantly with the incorporation of SiC reagent, which is 8.45%, 11.13%, and 13.37%, respectively, at 1550 °C, indicating that, the incorporation of SiC is beneficial to the recovery of Fe in the tempered slag.
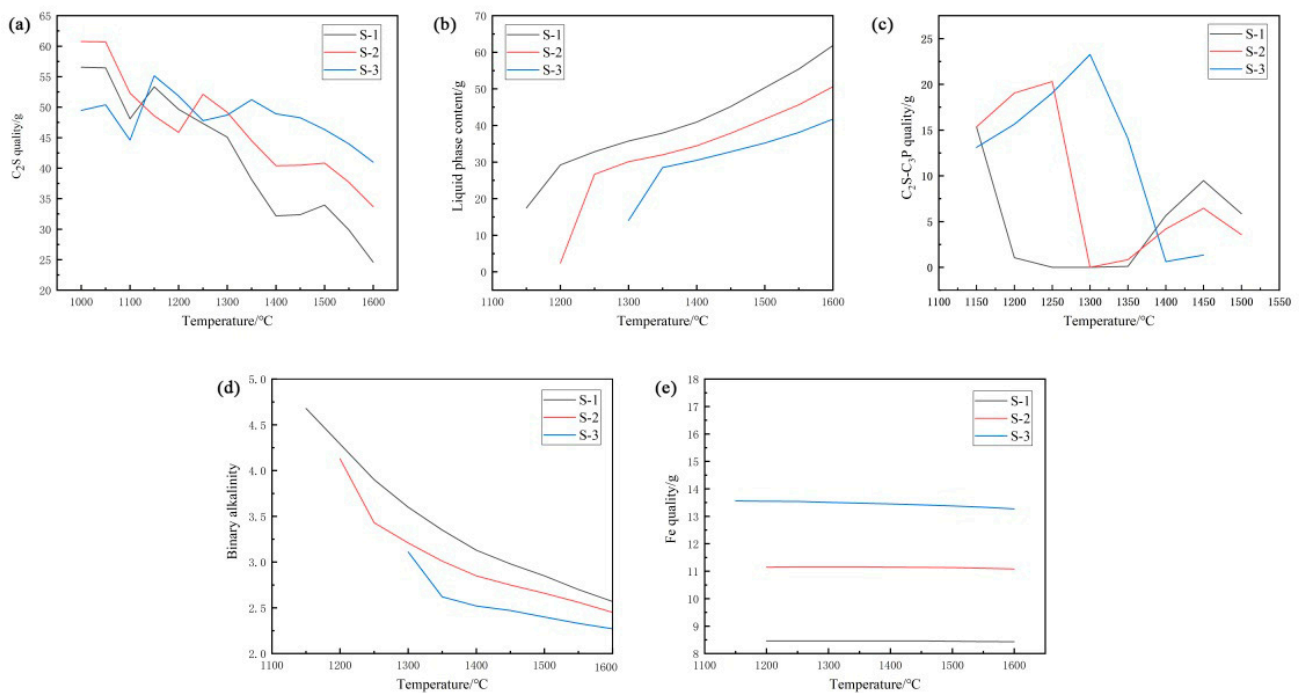

Figure 3. Equilibrium phase composition of tempered slag ((**a**–**e**) represent C_2S mass fraction, liquid mass fraction, C_2S-C_3P mass fraction, basicity, and Fe content, respectively).

In summary, if the self-powdering of tempering slag is realized, the content of P^{5+} in the tempering slag needs to be reduced. Combined with the changes of C_2S, C_2S-C_3P, and the amount of liquid phase in Figure 3, the experimental temperature should be higher than 1500 °C to cause P^{5+} to enter the liquid phase. According to the existing research, P^{5+} is easily combined with Fe and Mn in the liquid phase, and the content of P^{5+} in the tempering slag will be reduced in the form of iron alloy during the cooling process to achieve the double goal of "phosphorus removal and iron selection", and to create conditions for the self-powdering of tempering slag.

3.3. Microstructure and Mineral Composition of Tempered Slag

The tempered slag obtained from blast-furnace slag and SiC high-temperature molten reduction of tempered-steel slag was ground and analyzed by XRD diffractometer for its composition, and the results are shown in Figure 4. As can be seen from Figure 4, the physical phases of the tempered slag are magnesia–silica ($Ca_3Mg(SiO_4)_2$, C_3MS_2), $CaAl_3O_7$, albite ($Ca_7Mg(SiO_4)_4$, C_7MS_4), γ-C_2S, magnesia–olivine (Mg_2SiO_4, M_2S), and calcium–aluminum yellow feldspar ($Ca_2Al_2SiO_7$, C_2AS). The main diffraction peak in its XRD diffraction pattern is C_3MS_2, with the increase in SiC doping. The diffraction intensity of the main diffraction peak of C_3MS_2 at $2\theta = 33.52°$ is enhanced, indicating that the doping of SiC can promote the combination of C_2S and MgO in the tempered slag to form the olivine phase, and the magnesia–silica–calcite crystals are mostly plate-like structures with colorless, glassy luster and transparent bars, hardness of 3 and specific gravity of 2.48. The diffraction intensity of $CaAl_3O_7$ diffraction peaks at $2\theta = 31.40°$ and $52.08°$ is significantly enhanced, indicating that the doping of SiC can promote the combination of Ca^{2+} with Al_2O_3 in the tempered slag to form the $CaAl_3O_7$ phase. It has been confirmed that AlO^{2-} reacts easily with CO_2 and water vapor in air to produce calcium carbonate ($CaCO_3$) and aluminum hydroxide ($Al(OH)_3$) precipitates, which can provide a reference for theoretical studies on CO_2 adsorption by steel slag. The diffraction intensity of the γ-C_2S diffraction peak at $2\theta = 29.23°$ increases with the increase in SiC doping, and, combined with Figure 1, it is clear that the Figure 1b pulverization is the best. The analysis concluded that: due to the low content of C_2S in S-1, the cooling process is not enough to provide sufficient stress for the natural pulverization of the tempered slag; S-2 pulverization effect is the best, indicating that the stress of crystalline transformation of C_2S in the material phase during the cooling process can provide conditions for the pulverization of the tempered slag; and the main material phase composition after pulverization is C_3MS_2 and $CaAl_3O_7$. The chalking effect rate of S-3 is slightly lower than that of S-2. The analysis suggests that in S-3, the intensity of C_3MS_2 diffraction peak is significantly enhanced, and excessive C_3MS_2 minerals are generated, which are easy to agglomerate in the process of cooling, so that the stress generated by the C_2S crystallographic transformation cannot be uniformly distributed inside the specimen, and, therefore, local chalking occurs during the cooling of the specimen. As the blast-furnace slag is mixed in, the Al_2O_3 content in the tempered slag increases, and C_2AS with good thermal stability is formed during the roasting process, which has a melting point of 1593 °C and is often used in high-temperature ceramic colorants. The diffraction peaks of iron oxides and phosphorus oxides were not found in the XRD diffraction pattern. The analysis concluded that the reduced iron-alloy particles were not detected in the XRD diffraction pattern because of their high hardness, which was selected in the sample preparation process.

In order to further determine the physical composition and morphology of the tempered slag, as well as the attachment state of Fe, Mn, and P_2O_5, the microscopic morphology and regional elemental distribution of the S-1, S-2, and S-3 tempered slag specimens after roasting were analyzed using scanning electron microscopy, and the results are shown in Figures 5–7.
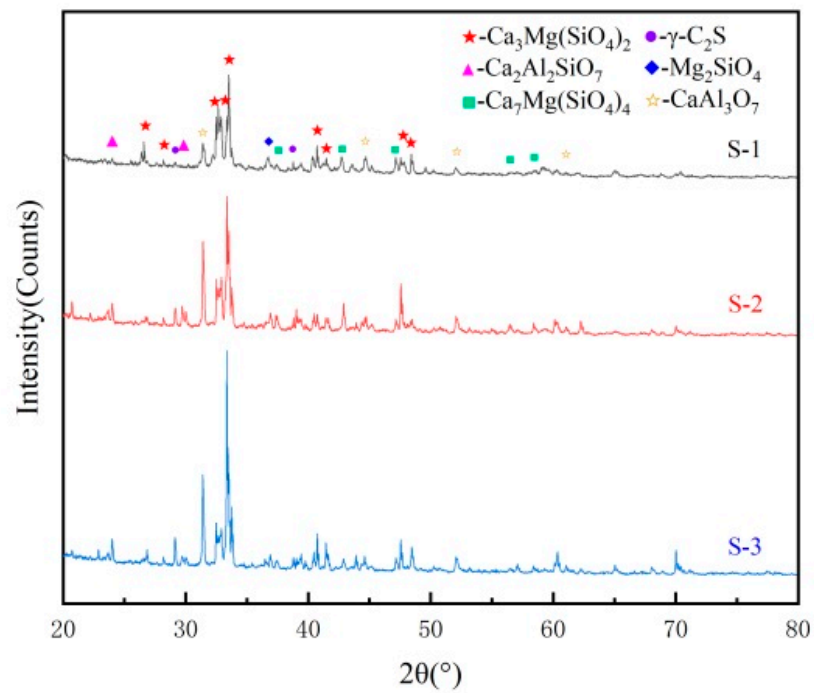
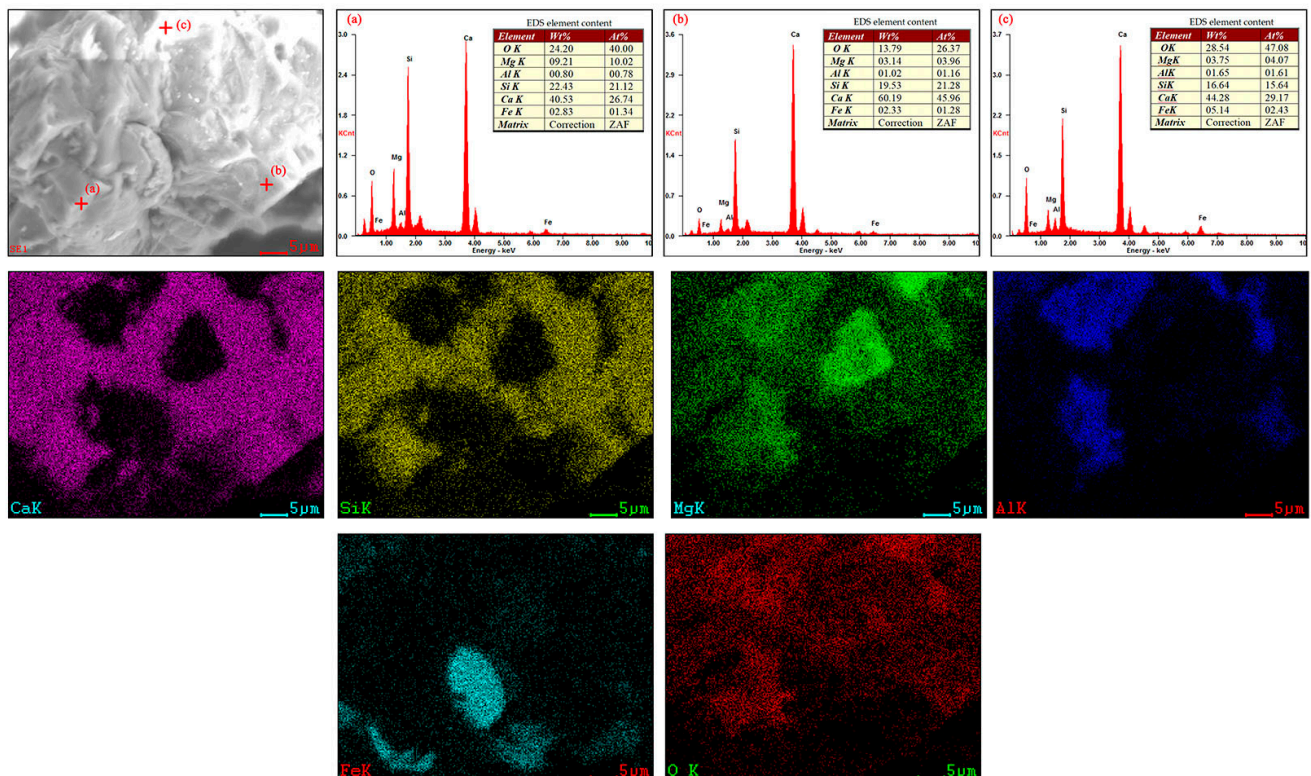**Figure 4.** XRD diffraction pattern of the tempered-slag specimen.

Figure 5. SEM morphology, face scan, and energy spectrum in S-1 (In the figure, "+" represents the position of the point, and "a–c" represents the corresponding sequence number).
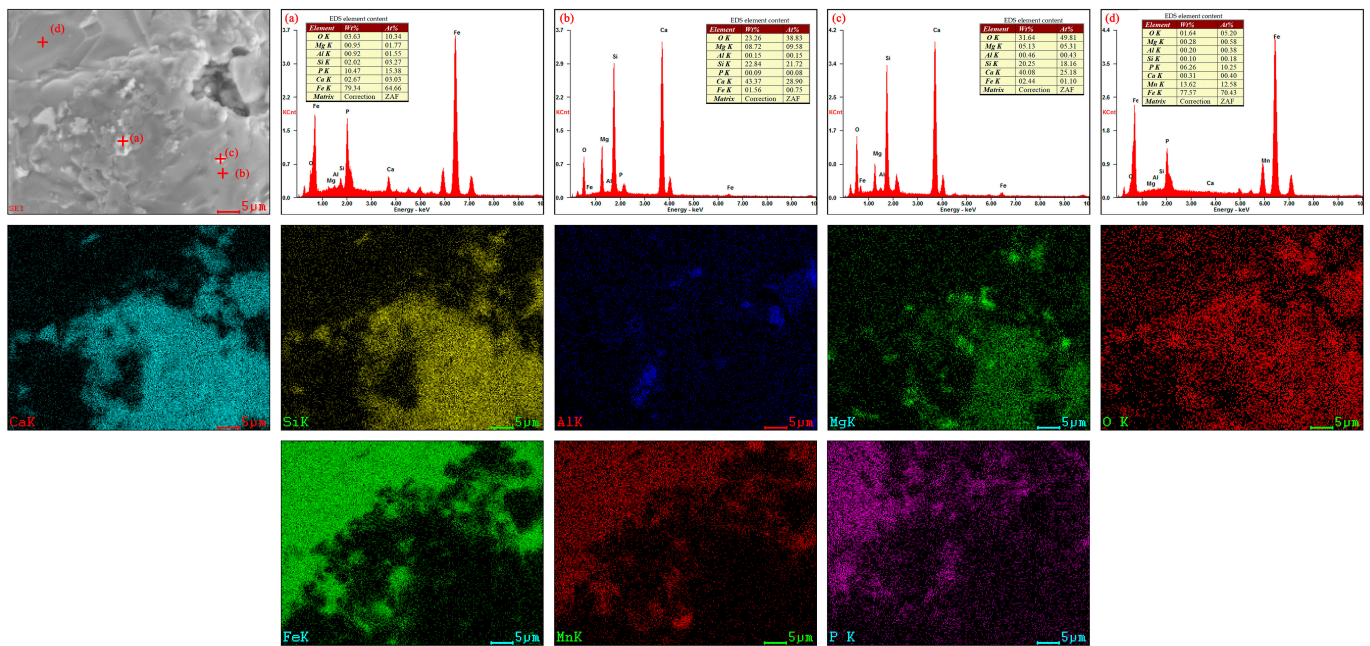
Figure 6. SEM morphology, face scan, and energy spectrum in S-2 (In the figure, "+" represents the position of the point, and "a–d" represents the corresponding sequence number).
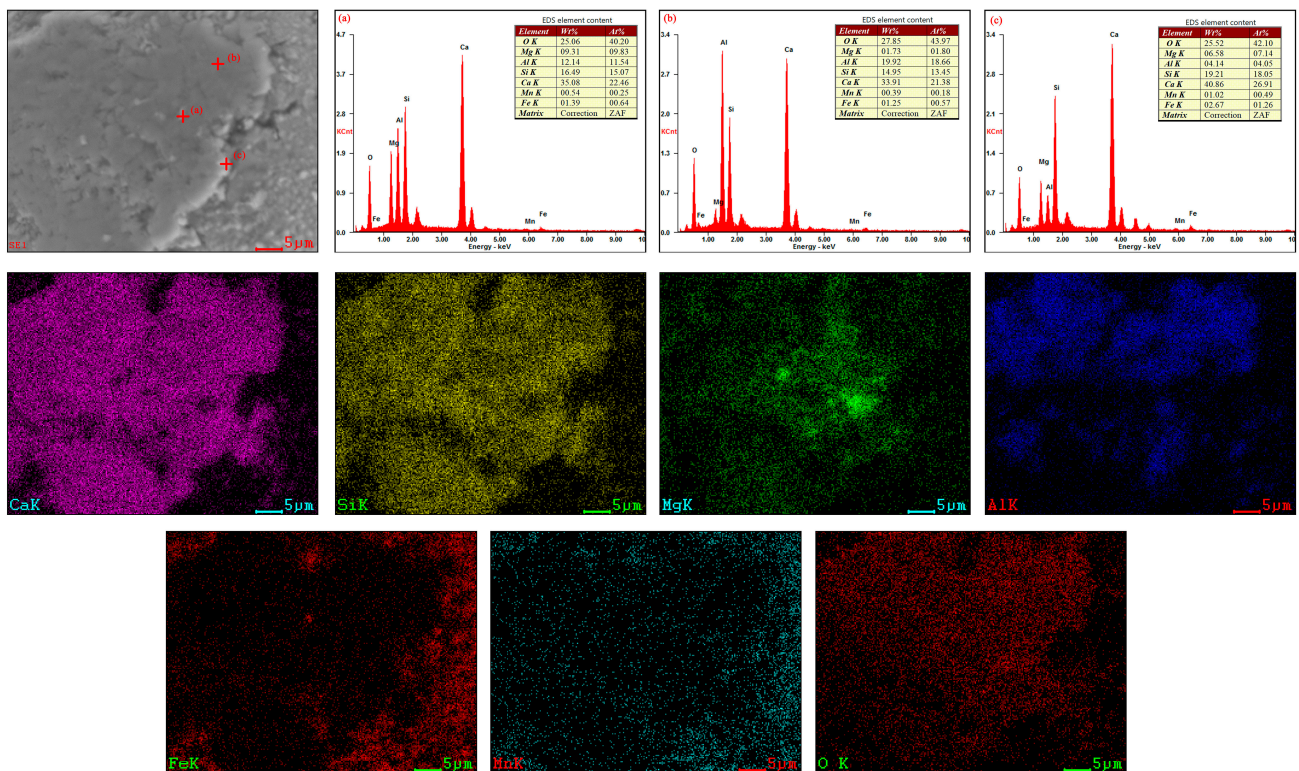

Figure 7. SEM morphology, face scan, and energy spectrum in S-3 (In the figure, "+" represents the position of the point, and "a–c" represents the corresponding sequence number).

In Figure 5, at point (a), the main elements are Ca, Si, and Mg with a molar ratio $n(Ca):n(Si):n(Mg) \approx 5:4:2$, which is similar to the molar ratio of the material phase in C_3MS_2 in XRD detection and it has a striped distribution, consistent with the characteristics of C_3MS_2. Combined with the element distribution pattern in the surface scan results, the

material phase at point (a) is considered to be C_3MS_2. At point (b), the main elements are Ca and Si, and their molar ratio is n(Ca):n(Si) $\approx$ 2.14:1. Combined with the element distribution law in the surface scan diagram, it is believed that point (b) is the C_2S phase. At point (c), the main elements are Ca, Si, and Mg, whose molar ratio n (Ca):n (Si) = 2:1, combined with the results of the distribution of elements in the surface scan that the physical phase of (c) is the same as at (b), and the different colors appear in the image, which, after analysis, is considered as being caused by poor electrical conductivity of the raw material. In addition, in the region to the left of point (c), elemental Al, elemental Mg, and elemental O are distributed and are thought to be present in this region in the form of Al_2O_3 and MgO. From the results of the surface scan, it can be seen that there is no other element distribution in the area of Fe distribution in the material phase, and it can be assumed that there is iron obtained by reduction in the material phase. The presence of P element was not detected in the face scan results, and it was considered that it did not show up during the face scan because it was enriched with C_2S and formed the C_2S-C_3P phase.

In Figure 6, at point (a), mainly Fe elements are dominant with some P elements, and its molar ratio is n(Fe):n(P) $\approx$ 4.1:1. Combining the thermodynamic calculation of the equilibrium state phase composition and the elemental distribution law in the results of the surface scan, it is considered that Fe_3P and Fe monomers are present at this point. This indicates that the combination of P and Fe under high-temperature conditions to form Fe3P did not decompose during the air-cooling process, achieving the purpose of dephosphorization, while the removal of P facilitated the self-powdering of the tempered slag during the cooling process, which is consistent with the conclusion that the self-powdering of S-2 occurred during the cooling process in Figure 1. Combined with the surface scan analysis, the C_3MS_2 phase at point (b) and the C_2S phase at point (c) are considered to be the main distributed elements at point (d), which are Fe, Mn, and P elements. The analysis combined with the thermodynamic equilibrium state phase composition suggests that the Fe alloys in this region are formed by Fe, Mn, and P. The recovery of Fe alloys in this tempered slag provides a theoretical basis. From the analysis of the face scan results, the main phases of S-2 are C_3MS_2 and Fe alloy, which complements the lack of detection of Fe alloy in the XRD diffraction pattern.

In Figure 7, at point (a), the main elemental compositions are Ca, Si, Al, and Mg. Combined with the elemental distribution in the surface scan, it can be assumed that the main phase compositions at this point are C_3MS_2 and C_2AS. The elemental molar ratio at point (b) is about n(Ca):n(Si):n(Al) $\approx$ 8:5:7, which is considered to be the C_2AS phase in combination with the elemental distribution law. The element distribution pattern in the face scan revealed that the Fe and Mn distribution regions in the S-3 specimen overlap, while no P element was found, so the region is considered to be an iron alloy containing Mn elements. Thermodynamic calculations show that the main phase of the tempered slag is C_2S, while the SEM and XRD diffraction results show C_3MS_2. The analysis suggests that the thermodynamic calculations are the composition of the phase in ideal equilibrium, while the actual experimental process does not reach the ideal equilibrium state, so this phenomenon will occur.

In summary, the main material phase in the tempering slag is C_3MS_2, C_2AS, and iron alloy, and the doping of 3% SiC reagent does not reduce the P_2O_5 content in the tempering slag to below 0.25%. Therefore, only partial pulverization of S-1 occurs internally during the cooling process, while the surface layer forms a hard crust. The complete pulverization of S-2 was achieved, indicating that the doping of 4% SiC reagent can effectively reduce the oxides of iron and manganese in the tempering slag to monomers and combine with the removed P, which is selected with the iron alloy, reducing the P_2O_5 content in the tempering slag to below 0.25%, achieving the purpose of iron selection and dephosphorization, and creating favorable conditions for the self-powdering of the tempering slag. Doping with 5% SiC reagent, a local caking phenomenon, considering the high proportion of SiC reagent, increased the internal temperature of the specimen, providing favorable conditions for the carbonization reaction of C_2S. The carbonization products are $CaCO_3$ and highly

polymerized SiO_2 gel, increasing the stability of the C_2S crystalline form, so this part of the specimen is not completely pulverized.

The mineral phase assay was performed for the Fe beads in the S-2 experimental product, and the results are shown in Figure 8. From the figure, it can be seen that the Fe phase contains more C, Mn, and P elements at this time. The results of the surface scan showed that the P element was distributed in a "dot" pattern, and the analysis suggested that the relative content of Mn and Fe was higher in the area with high P content. S-2 ferroalloys with high Mn and P content can be considered for use as raw materials for high P steels or Fe–Mn alloy steels.
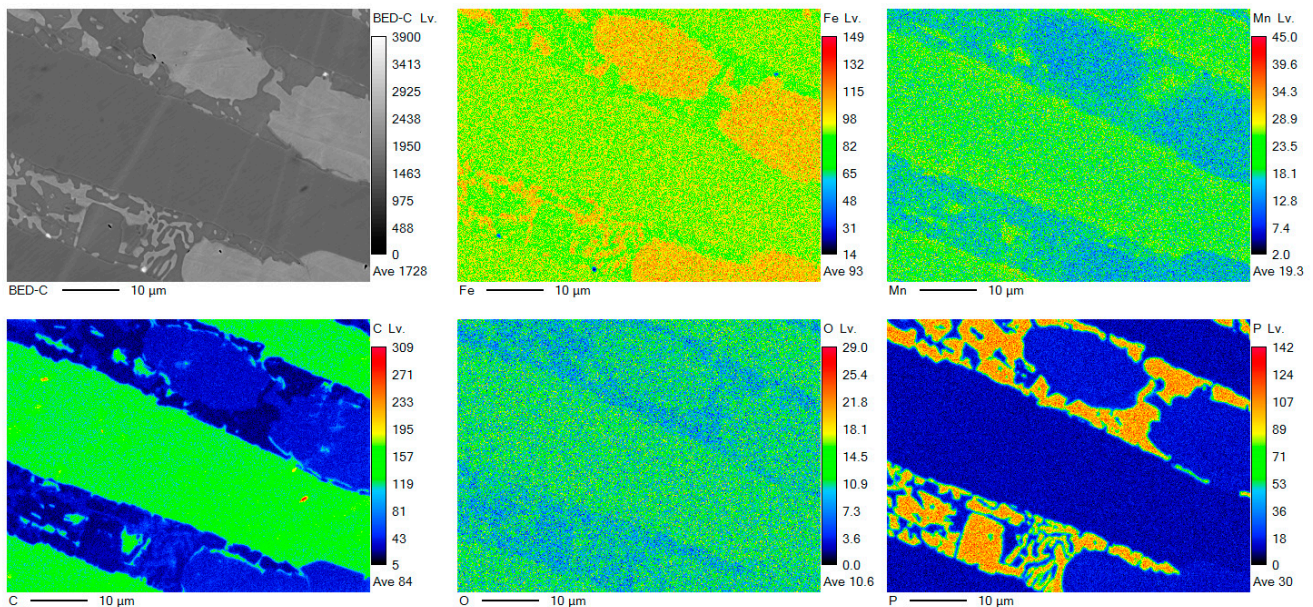
Figure 8. S-2 electron probe field emission scanning pattern.

4. Conclusions

High melting point SiC (>2700 °C) is not easy to burn with a loss under high-temperature conditions, and can be used as an effective reducing agent and modifier. At the same time, SiC blending can reduce the basicity of tempering slag, creating conditions for the self-powdering of tempering slag. The main phases of the tempered slag after roasting were magnesia–silica calcium ($Ca_3Mg(SiO_4)_2$, C_3MS_2), calcium–aluminum yellow feldspar ($Ca_2Al_2SiO_7$, C_2AS), γ-C_2S, and iron alloy.

Doping with 4% SiC reagent, on the one hand, can cause tempering slag in the air-cooling process to lead to self-powdering, reducing the cost of tempering slag crushing; on the other hand, reducing metal oxides in tempering slag to form ferroalloys and removing ferroalloys in the phosphorus of tempering slag achieves the same purpose of blast-furnace slag and, hence, leads to steel slag "resource utilization".

Thermodynamic analysis reveals: during P^{5+} solid solution to C_2S and the formation of C_2S-C_3P in the temperature range of 1150~1250 °C, the experimental temperature is higher than 1500 °C, there is the formation of a large number of liquid phases, kinetic conditions are improved and more conducive to P^{5+}, and the liquid phases of Fe and Mn are combined to form an alloy and reduce the content of P^{5+} in the tempering slag to create conditions for the self-powdering of tempering slag. The liquid-phase line temperatures of 3%, 4%, and 5% SiC doping reagents were 1150 °C, 1200 °C, and 1300 °C, respectively, and the basicity in the liquid phase was 4.68, 4.13, and 3.10, respectively, indicating that the doping of SiC reagents could increase the liquid-phase line temperature and decrease the binary basicity in the liquid phase.

References

1. Sun, Z.F.; Ren, X.; Peng, F. Current situation and prospect of comprehensive utilization of bulk solid waste in iron and steel industry. *Metall. Manag.* **2022**, *450*, 39–43.
2. Su, C.Y.; Li, X.Y.; Lin, Y. The path of green, low-carbon and high-quality development of solid waste in the iron and steel industry. *Sintered Pellets* **2022**, *47*, 7.
3. Wang, S. Study on the Application of High Titanium Slag-Steel Slag-Silica Fume Composite Mineral Admixture in Concrete. Master's Thesis, Southwest University of Science and Technology, Mianyang, China, 2021.
4. Liu, X.; Wang, D.Z.; Li, Z.W.; Ouyang, W.; Bao, Y.P.; Gu, C. Efficient separation of iron elements from steel slag based on magnetic separation process. *J. Mater. Res. Technol.* **2023**, *23*, 2362–2370. [CrossRef]
5. Zhao, J.H.; Li, Z.H.; Wang, D.M.; Yan, P.Y.; Luo, L.; Zhang, H.W.; Zhang, H.M.; Gu, X.B. Hydration superposition effect and mechanism of steel slag powder and granulated blast furnace slag powder. *Constr. Build. Mater.* **2023**, *366*, 130101. [CrossRef]
6. Zhou, Z.G.; Yang, H.Z.; Ai, L.Q.; Wang, S.H.; Hu, J.H.; Chen, H. Research status and prospect of recycling technology of steel slag containing phosphorus in converter. *Steel* **2021**, *56*, 22–39.
7. Hao, S.; Luo, G.P.; Lu, Y.Y.; Chai, Y.F.; Song, W.; An, S.L. Status and prospects of steel slag modification and carbon sequestration research. *Sintered Pellets* **2022**, *47*, 31–38.
8. Hao, S.; Luo, G.P.; Chen, Y.S.; Chai, Y.F.; Song, W.; An, S.L. Effect of phosphorus-aluminum compounding on C_2S crystallographic transformation. *China Metall.* **2022**, *32*, 126–133.
9. Pyzalski, M.; Dąbek, J.S.; Adamczyk, A.; Brylewski, T. Physicochemical Study of the Self-Disintegration of Calcium Orthosilicate ($\beta \rightarrow \gamma$) in the Presence of the $C_{12}A_7$ Aluminate Phase. *Materials* **2021**, *14*, 6459. [CrossRef] [PubMed]
10. Ahmed, A.; Abubakr, P.; Salih, M.A. Efficient models to evaluate the effect of C_3S, C_2S, C_3A, and C_4AF contents on the long-term compressive strength of cement paste. *Structures* **2023**, *47*, 1459–1475. [CrossRef]
11. Li, Y.; Xiong, Y.D.; Zang, Y.G.; Chen, H.T.; Yan, L.X.; Yu, Y.W. Study on Properties of Cold Bonded Briquettes Prepared from Return Fines of Sinter. *Steel Res. Int.* **2022**, *93*, 2200304. [CrossRef]
12. Bhatt, R.T.; Eldridge, J.I. Heat treatment effects on microstructure and properties of CVI SiC/SiC composites with Sylramic™-iBN SiC fibers. *J. Eur. Ceram. Soc.* **2023**, *43*, 2376–2387. [CrossRef]
13. Mu, Y.D.; Liu, Z.C.; Wang, F.Z. Kinetics of γ-type dicalcium silicate carbonation reaction. *J. Silic.* **2022**, *50*, 457–465.